J|A|C|S
ARTICLES

Published on Web 07/22/2008

Comprehensive Mechanism and Structure-Sensitivity of Ethanol Oxidation on Platinum: New Transition-State Searching Method for Resolving the Complex Reaction Network

Hui-Fang Wang and Zhi-Pan Liu*

Shanghai Key Laboratory of Molecular Catalysis and Innovative Materials, Department of Chemistry, Fudan University, Shanghai, China 200433

Received March 5, 2008; E-mail: zpliu@fudan.edu.cn

Abstract: Ethanol oxidation on Pt is a typical multistep and multiselectivity heterogeneous catalytic process. A comprehensive understanding of this fundamental reaction would greatly benefit design of catalysts for use in direct ethanol fuel cells and the degradation of biomass-derived oxygenates. In this work, the reaction network of ethanol oxidation on different Pt surfaces, including close-packed Pt{111}, stepped Pt{211}, and open Pt{100}, is explored thoroughly with an efficient reaction path searching method, which integrates our new transition-state searching technique with periodic density functional theory calculations. Our new technique enables the location of the transition state and saddle points for most surface reactions simply and efficiently by optimization of local minima. We show that the selectivity of ethanol oxidation on Pt depends markedly on the surface structure, which can be attributed to the structure-sensitivity of two key reaction steps: (i) the initial dehydrogenation of ethanol and (ii) the oxidation of acetyl (CH_3CO). On open surface sites, ethanol prefers C−C bond cleavage via strongly adsorbed intermediates (CH_2CO or CHCO), which leads to complete oxidation to CO_2. However, only partial oxidizations to CH_3CHO and CH_3COOH occur on Pt{111}. Our mechanism points out that *the open surface Pt{100} is the best facet to fully oxidize ethanol at low coverages*, which sheds light on the origin of the remarkable catalytic performance of Pt tetrahexahedra nanocrystals found recently. The physical origin of the structure-selectivity is rationalized in terms of both thermodynamics and kinetics. Two fundamental quantities that dictate the selectivity of ethanol oxidation are identified: (i) the ability of surface metal atoms to bond with unsaturated C-containing fragments and (ii) the relative stability of hydroxyl at surface atop sites with respect to other sites.

1. Introduction

"How to selectively activate a chemical bond to make a desired product" must rank the top concern in chemistry. A direct ethanol fuel cell (DEFC), as a good example, features ethanol oxidation on an anode to deliver clean, abundant, and reliable energy. While the conversion of ethanol to CO_2 is regarded as the key to the DEFC performance,[1,2] extensive studies in both academia and industry revealed that it is very challenging to fully oxidize ethanol on Pt-based anodes due to the presence of partial-oxidation channels.[3,4] Apart from its application in fuel cells, ethanol oxidation is often regarded as the model system to understand the degradation of high-molecular-weight oxygenates, such as biomass-derived carbohydrates[5] (e.g., glucose and sorbitol). To design a catalyst to degrade these natural products to make hydrogen or syngas is again of profound interests. Aiming to shed light on the mechanism of ethanol oxidation, this work develops a fast transition state location technique to explore the whole reaction network of ethanol oxidation on different structured Pt surfaces from first principles. The general patterns as well as the surface-structure dependence during the successive bond activations are revealed and rationalized from the atomic level.

The electro-oxidation of ethanol has been examined on many anode materials, and platinum was revealed to be the most catalytically active for ethanol C−C bond cleavage.[6–9] While the overall mechanism of oxidation remains uncertain, modern experimental techniques such as differential electrochemical mass spectrometry[6,7,10–12] and *in situ* infrared reflectance spectroscopy[13–15] have helped to identify many

(1) Demirci, U. B. *J. Power Sources* **2007**, *169*, 239.
(2) Antolini, E. *J. Power Sources* **2007**, *170*, 1.
(3) Vigier, F.; Rousseau, S.; Coutanceau, C.; Leger, J. M.; Lamy, C. *Top. Catal.* **2006**, *40*, 111.
(4) Vigier, F.; Coutanceau, C.; Perrard, A.; Belgsir, E. M.; Lamy, C. *J. Appl. Electrochem.* **2004**, *34*, 439.
(5) Davda, R. R.; Shabaker, J. W.; Huber, G. W.; Cortright, R. D.; Dumesic, J. A. *Appl. Catal., B* **2005**, *56*, 171.
(6) Gootzen, J. F. E.; Visscher, W.; vanVeen, J. A. R. *Langmuir* **1996**, *12*, 5076.
(7) Schmidt, V. M.; Ianniello, R.; Pastor, E.; Gonzalez, S. *J. Phys. Chem.* **1996**, *100*, 17901.
(8) Wang, Q.; Sun, G. Q.; Jiang, L. H.; Xin, Q.; Sun, S. G.; Jiang, Y. X.; Chen, S. P.; Jusys, Z.; Behm, R. J. *Phys. Chem. Chem. Phys.* **2007**, *9*, 2686.
(9) Wang, H.; Jusys, Z.; Behm, R. J. *Fuel Cells* **2004**, *4*, 113.
(10) Ianniello, R.; Schmidt, V. M.; Rodriguez, J. L.; Pastor, E. *J. Electroanal. Chem.* **1999**, *471*, 167.
(11) Colmenares, L.; Wang, H.; Jusys, Z.; Jiang, L.; Yan, S.; Sun, G. Q.; Behm, R. J. *Electrochim. Acta* **2006**, *52*, 221.
(12) Wang, H.; Jusys, Z.; Behm, R. J. *J. Phys. Chem. B* **2004**, *108*, 19413.

10.1021/ja801648h CCC: $40.75

common oxidation intermediates. CH_3COH, CH_3CO, CH_x, and CO are the most abundant surface intermediates over polycrystalline Pt, while CH_3CHO, CH_3COOH, and CO_2 are the three major products detected. The low efficiency of DEFCs was often interpreted as a result of partial oxidations to CH_3CHO and CH_3COOH, since it is difficult to further oxidize CH_3COOH at typical fuel cell anode conditions (e.g., below 0.65 V vs NHE). It remains puzzling why partial oxidation always dominates and what prevents the further oxidation of CH_3CHO and CH_3COOH.

To improve the cell performance, recent studies have been focused on modifying pure Pt catalyst via two possible means. Perhaps the most popular method is to alloy Pt with a second and even a third metal. Typical additives include Sn,[11,16–18] Ru,[8,19,20] Rh,[21,22] W,[23] Pd,[24] Os,[25] and so on. It was reported that the best binary catalyst is Pt−Sn, although its activity for total oxidation of ethanol to CO_2 is actually much worse than that of Pt alone. The alloying with Sn appears to suppress the production of CH_3CHO and CO_2 but increase the selectivity to CH_3COOH.[3,4,17,26,27] The other method, which appears more promising, involves modification of the Pt surface structure. For example, Tarnowski et al.[28] compared ethanol electro-oxidation on Pt{111}, Pt{557}, and Pt{335} and found that the selectivity to acetic acid is markedly lower on the stepped surfaces. In methanol electro-oxidation on Pt, the selectivity was also found to be sensitive to the surface structure of Pt.[29] A recent experiment by Tian et al.[30] made further progress by preparing platinum nanocrystals that expose only open {100} terraces and a large density of monatomic steps. This new material was reported to exhibit good catalytic activity in ethanol electro-oxidation.The dramatic effects of surface structures on selectivity are apparently unanticipated and add more question marks in the field.

Apart from electrochemistry studies, ethanol oxidization has also been carried out on a group of transition metal surfaces using surface science techniques, including Rh{111},[31] Pd{111}[32] and {110},[33] Ir{111},[34] and so on. Compared to the large volume of experimental work, theoretical studies on ethanol oxidation are limited. Alcala et al. first calculated selected surface species derived from ethanol on Pt{111}[35] and Pt_3Sn{111}[36] using density functional theory (DFT). From the thermodynamics rule, they deduced that the ketenyl (CHCO) species may be the precursor for C−C bond-breaking, which needs to overcome a reaction barrier of 0.95 eV. Considering that C_1 products from ethanol are observed below 300 K in surface science experiments[2] and that CO_2 is identified even at low electrical potentials in electro-chemical experiments,[7,37] the DFT results on the high barrier to C−C bond cleavage were questioned. Vesselli et al.[38] thus investigated ethanol decomposition on Pt{111} within the framework of the semiempirical unity bond index−quadratic exponent potential (UBI-QEP) approach and found more reasonable energetics. To date, there is no agreement regarding where and how ethanol breaks into C_1 species, the essential step toward total oxidation. Considering that C−C bond cleavage and thus CO_2 formation can occur at mild conditions (implying overall low kinetic barriers), it is quite peculiar why the selectivity to CO_2 is the lowest among the three main products (CO_2, CH_3CHO, and CH_3COOH).

To fully resolve the puzzles, a complete kinetic description of ethanol oxidation on Pt from first principles is desired. Exploration of the whole reaction network is, however, a formidable task, not least because ethanol has more than 40 possible oxidative derivatives, each of which contains many types of chemical bonds (C−C, C−O, O−H, and several types of C−H bonds). Even with the advent of first-principle DFT total energy calculations, such studies for surface reactions are very challenging due to the limitation of current reaction path searching methods in locating the transition state (TS) of surface reactions. In this work, we developed a new version of the constrained-minimization technique, named the constrained Broyden minimization, which simplifies the TS location for complex surface reactions with a significant speed-up in convergence. The new method allowed us to study explicitly all the likely reaction pathways on three common Pt surfaces within the self-consistent DFT framework. The whole reaction map was obtained, which helps to rationalize the long-standing puzzles in the field and provides important clues for the design of better anode catalysts for ethanol oxidation.

2. Theoretical Methodology

2.1. Density Functional Theory Calculations. All DFT calculations were performed with the SIESTA package using numerical atomic orbital basis sets and Troullier−Martins norm-conserving pseudopotentials[39] (scalar relativistic for heavy elements). The exchange-correlation functional used was the generalized gradient approximation method, known as GGA-PBE. The other details of

(13) Hitmi, H.; Belgsir, E. M.; Leger, J. M.; Lamy, C.; Lezna, R. O. *Electrochim. Acta* **1994**, *39*, 407.
(14) Beden, B.; Morin, M.-C.; Hahn, F.; Lamy, C. *J. Electroanal. Chem.* **1987**, *229*, 353.
(15) Chang, S. C.; Leung, L. W. H.; Weaver, M. J. *J. Phys. Chem.* **1990**, *94*, 6013.
(16) Wang, H.; Jusys, Z.; Behm, R. J. *J. Power Sources* **2006**, *154*, 351.
(17) Rousseau, S.; Coutanceau, C.; Lamy, C.; Leger, J. M. *J. Power Sources* **2006**, *158*, 18.
(18) Mann, J.; Yao, N.; Bocarsly, A. B. *Langmuir* **2006**, *22*, 10432.
(19) Fujiwara, N.; Friedrich, K. A.; Stimming, U. *J. Electroanal. Chem.* **1999**, *472*, 120.
(20) Camara, G. A.; de Lima, R. B.; Iwasita, T. *Electrochem. Commun.* **2004**, *6*, 812.
(21) Sen Gupta, S.; Datta, J. *J. Electroanal. Chem.* **2006**, *594*, 65.
(22) de Souza, J. P. I.; Queiroz, S. L.; Bergamaski, K.; Gonzalez, E. R.; Nart, F. C. *J. Phys. Chem. B* **2002**, *106*, 9825.
(23) Zhou, W. J.; Li, W. Z.; Song, S. Q.; Zhou, Z. H.; Jiang, L. H.; Sun, G. Q.; Xin, Q.; Poulianitis, K.; Kontou, S.; Tsiakaras, P. *J. Power Sources* **2004**, *131*, 217.
(24) Zhou, W. J.; Zhou, Z. H.; Song, S. Q.; Li, W. Z.; Sun, G. Q.; Tsiakaras, P.; Xin, Q. *Appl. Catal. B−Environ.* **2003**, *46*, 273.
(25) Santos, V. P.; Del Colle, V.; de Lima, R. B.; Tremiliosi, G. *Electrochim. Acta* **2007**, *52*, 2376.
(26) Antolini, E. *Appl. Catal. B−Environ.* **2007**, *74*, 337.
(27) Wu, G.; Swaidan, R.; Cui, G. F. *J. Power Sources* **2007**, *172*, 180.
(28) Tarnowski, D. J.; Korzeniewski, C. *J. Phys. Chem. B* **1997**, *101*, 253.
(29) Cao, D.; Lu, G. Q.; Wieckowski, A.; Wasileski, S. A.; Neurock, M. *J. Phys. Chem. B* **2005**, *109*, 11622.
(30) Tian, N.; Zhou, Z. Y.; Sun, S. G.; Ding, Y.; Wang, Z. L. *Science* **2007**, *316*, 732.
(31) Houtman, C. J.; Barteau, M. A. *J. Catal.* **1991**, *130*, 528.
(32) Davis, J. L.; Barteau, M. A. *Surf. Sci.* **1990**, *235*, 235.
(33) Shekhar, R.; Barteau, M. A.; Plank, R. V.; Vohs, J. M. *J. Phys. Chem. B* **1997**, *101*, 7939.
(34) Weststrate, C. J.; Ludwig, W.; Bakker, J. W.; Gluhoi, A. C.; Nieuwenhuys, B. E. *ChemPhysChem* **2007**, *8*, 932.
(35) Alcala, R.; Mavrikakis, M.; Dumesic, J. A. *J. Catal.* **2003**, *218*, 178.
(36) Alcala, R.; Shabaker, J. W.; Huber, G. W.; Sanchez-Castillo, M. A.; Dumesic, J. A. *J. Phys. Chem. B* **2005**, *109*, 2074.
(37) Shin, J. W.; Tornquist, W. J.; Korzeniewski, C.; Hoaglund, C. S. *Surf. Sci.* **1996**, *364*, 122.
(38) Vesselli, E.; Coslovich, G.; Comelli, G.; Rosei, R. *J. Phys. Condens. Matter* **2005**, *17*, 6139.
(39) Soler, J. M.; Artacho, E.; Gale, J. D.; Garcia, A.; Junquera, J.; Ordejon, P.; Sanchez-Portal, D. *J. Phys. Condens. Matter* **2002**, *14*, 2745.

DFT calculations using SIESTA can be found elsewhere.[40] All the metal surfaces were modeled with four-layer slabs, with the top two layers being relaxed. The Pt{111}, Pt{211}, and Pt{100} surfaces are modeled by $p(4\times4)$, $p(3\times1)$, and $p(3\times3)$ unit cells, respectively. To further check the accuracy of the calculated reaction barriers, some key reaction steps were also examined with the plane-wave methodology as implemented in CASTEP package,[41] which show good consistency (the difference in barriers was within 0.1 eV). All TSs were located using the new constrained Broyden minimization technique as addressed below, which significantly speeds up the searching for reaction paths. For the important reactions, vibrational frequency calculations were performed to validate the TS and to calculate the zero-point energy (ZPE) where correction to the reaction barrier is necessary.

To compare the stability of reaction intermediates, we defined the adsorption energies (E_X) of a hydrocarbon oxygenate X ($C_xH_yO_z$) with respect to the gas-phase ethanol, the adsorbed OH, and the adsorbed H by writing $C_xH_yO_z$ as $x/2(C_2H_6O) + (y - 3x)H + (z - x/2)O$. The computation can be done with eq 1,

$$E_X = E_{X/sur} - E_{sur} - \left[\frac{x}{2}E_e + (y-3x)(E_H - E_{sur}) + \left(z-\frac{x}{2}\right)(E_{OH} - E_H)\right] \quad (1)$$

where E_e, E_{OH}, E_H, and E_{sur} are the DFT total energies of the gas-phase ethanol, the adsorbed OH, the adsorbed H, and the bare surface, respectively.

2.2. Our Transition-State Searching Method: Constrained Broyden Minimization Technique. The constrained minimization method is perhaps the most intuitive method for locating TSs, which searches for TSs from a guessed TS-like structure by fixing only one degree of freedom, e.g., the distance of the dissociating chemical bond.[42] In practice, the implementation of the method has two technique problems: (i) It is difficult mathematically to implement the constraint in more efficient but sophisticated optimization methods, such as the quasi-Newon−Broyden method involving the inverse Jacobian matrix.[43–45] (ii) It is also hard to update the constraint "on-the-fly", for which the direction for update is required, because to follow the negative modes through the computation of an exact Hessian requires great effort and is practically not available for DFT calculations with non-Gaussian-orbital basis. For these reasons, the constrained minimization method is most used for simple reactions, enforcing the constraint in robust first-order structure optimization methods (e.g., conjugate-gradient method), and the constraint is often manually varied by carrying out separate runs, for example, to fix the distance of a dissociating bond at selected consecutive distances, e.g., 1.6, 1.8, 2.0 Å and so on.

In this work, we developed a new version of the constrained minimization method, which is designed to inherit the advantages of Broyden optimization in finding the local minimum.[43–45] In the method, we impose the constraint right after each Broyden geometry optimization step, and we also update the constraint progressively toward the true TS during a single optimization. The Jacobian matrix of the Broyden method is forced to reset once the constraint is updated. This means that our TS optimization (a single run) is equivalent to a sequence of many individual runs, each inheriting a better guessed TS-like structure from the last run. The detail for a bond-distance fixation, as implemented in this work, is described as follows.

To constrain the distance between an atomic pair A and B, eqs 2−7 are used to determine the new positions ($r_{A'}$ and $r_{B'}$) of the constrained atoms after each Broyden step.

$$d_N = r_A - r_B \quad (2)$$

$$\lambda = (F_A - F_B)/(F_A + F_B) \quad (3)$$

$$r_{A'} = (r_A + r_B)/2 + (\lambda + d_t/d_N - \lambda d_t/d_N)(r_A - r_B)/2 \quad (4)$$

$$r_{B'} = (r_A + r_B)/2 + (\lambda - d_t/d_N - \lambda d_t/d_N)(r_A - r_B)/2 \quad (5)$$

$$d_t = r_{A'} - r_{B'} \quad (6)$$

$$d_t^{pred} = d_t - \beta(d_N - d_t) \quad (7)$$

where the predicted new positions of A and B and their distance after each Broyden step are r_A, r_B, and d_N, respectively; d_t is the fixed (target) distance that should be imposed; F_A and F_B are the root-mean-square forces on atoms A and B, respectively; λ is a conditional parameter, ranging from -1 ($F_A \ll F_B$) to $+1$ ($F_A \gg F_B$), which allows for the atom with larger force to be less constrained [as λ is close to $1/-1$, almost no constraint is imposed on atom A/B ($r_{A'} \approx r_A/r_{B'} \approx r_B$)]. We call the implementation of λ "treatment 1".

The distance between the constrained atoms (d_t) can be updated to d_t^{pred} using eq 7. As Broyden optimization points to the local minimum on the potential energy surface, the direction of the distance change provided by Broyden method (i.e., $d_N - d_t$) is, in fact, opposite to that should be updated (i.e., $d_t^{pred} - d_t$) in order to find TS, a saddle point on the potential energy surface. The parameter β (>0) is used for damping the distance change, and in practice it can be optimized by taking into account information from several historical runs. Once an update is done (d_t is changed to d_t^{pred}), we take the following two actions: (i) the Jacobian matrix is reset and (ii) the positions of all atoms neighboring A and B (the first and second neighbors) are adjusted accordingly to provide a better-guessed TS-like geometry. The adjustment of the neighboring groups is called "treatment 2" (see Supporting Information for an illustration of TS-searching trajectories with and without treatments 1 and 2). The constrained Broyden optimization should then be carried out at the fixed new d_t for a few more steps to relax all the other degrees of freedom. By this iterative approach, d_t will oscillate around and eventually converge to that of the true TS when all the forces on atoms vanish. The validity of the approach has been proved by vibrational frequency calculations in typical reactions, showing one and only one negative mode at the located TS.

3. Results

3.1. Reaction Network of Ethanol Oxidation on Pt Surfaces. To investigate the surface structural effects on ethanol oxidation, we considered the three most common types of Pt surfaces, namely, the closed-packed {111} surface, the monatomic steps as represented by Pt{211}, and the open {100} surface (unreconstructed, square lattice). We initiated our investigations by finding the key reaction steps on Pt{111} to gather a general view of the reaction process; next, we examined the other two, less stable surfaces to verify whether these special structures will modify the activity. To map out the whole reaction network, we took a recursive "trial-and-error" approach, the high work load of which is largely eased by the new contrained Broyden minimization technique. We first explored the initial bond cleavage of ethanol by breaking its CH, OH, and CC bonds individually and then walked through each "likely" oxidation channel stepwise until C_1 species were reached. By "likely", we mean that the reaction route must have relatively low reaction barriers, typically below 0.75 eV (a magnitude regarded as surmountable for reactions occurring at

(40) Wang, C. M.; Fan, K. N.; Liu, Z. P. *J. Am. Chem. Soc.* **2007**, *129*, 2642.
(41) Payne, M. C.; Teter, M. P.; Allan, D. C.; Arias, T. A.; Joannopoulos, J. D. *Rev. Mod. Phys.* **1992**, *64*, 1045.
(42) Liu, Z. P.; Hu, P. *Top. Catal.* **2004**, *28*, 71.
(43) Johnson, D. D. *Phys. Rev. B* **1988**, *38*, 12807.
(44) Kresse, G.; Furthmuller, J. *Comput. Mater. Sci.* **1996**, *6*, 15.
(45) Broyden, C. G. *Math. Comput.* **1965**, *19*, 557.

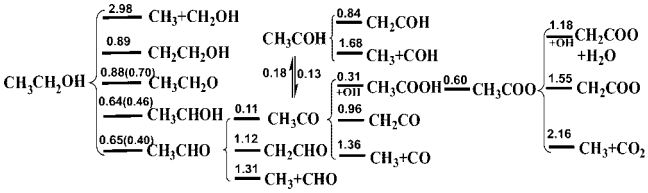

Figure 1. Calculated reaction network and reaction barriers (units, eV) for ethanol oxidation on Pt{111}. H atoms produced were omitted for clarity. The data in parentheses are the barriers after the zero-point-energy correction.

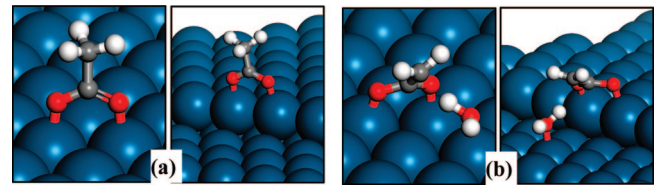

Figure 2. (a) Geometries of adsorbed acetate on Pt{111} and {211}. (b) Transition-state structures for the reaction $CH_3COO + OH \rightarrow CH_2COO + H_2O$ on Pt{111} and {211}, which are the lowest energy channels to oxidize acetate.

room temperatures). In deducing a complete oxidation mechanism, we also took into account the participation of oxidative species such as hydroxyl, considering that the applied anode potential for ethanol electro-oxidation is in the range of 0−0.8V vs NHE,[2,30] where the higher potential end (e.g., above 0.5 V[46,47]) favors the formation of adsorbed hydroxyls and adsorbed O species. In the following, we elaborate on our calculated reaction networks for ethanol oxidation on the three surfaces.

3.1.1. Pt{111}. The calculated reaction network on Pt{111} is schematically summarized in Figure 1. A few key elementary steps in the map have been studied in our recent work, where a smaller unit cell ($p(2\times2)$ Pt{111}) for reactions was utilized.[48] Here we aimed at establishing a complete reaction map with particular emphasis on C−C bond cleavage. As a starting point, we identified five different bond-breaking pathways for the initial bond cleavage of ethanol. C−C bond-breaking is most unlikely, with an extremely high reaction barrier (2.98 eV), and the next most unfavorable pathway is β-dehydrogenation. While the high barriers of these two pathways may be expected, it is quite unanticipated to observe that hydroxyl dehydrogenation (named as *the OH path* hereafter) is, in fact, less favorable than dehydrogenations involving α-H. α-Dehydrogenation (named as *the CH path* hereafter) and the one-step concerted dehydrogenation to acetaldehyde (CH_3CHO) (named as *the concerted path* hereafter) are the pathways with the lowest barriers, which were first identified in our recent work.[48] The concerted path features a TS with two in-dissociating hydrogen atoms standing at atop sites of Pt and the left CH_3CHO fragment flying over the two H's. After the ZPE correction, the concerted path has a reaction barrier 0.06 eV lower than that of the α-dehydrogenation path. Because the concerted path produces directly the weakly adsorbed acetaldehyde that is ready for desorption from the surface, the theoretical results provide an atomic-level rationalization for the observed high selectivity to acetaldehyde for ethanol electro-oxidation on Pt catalysts.[3]

As long as the acetaldehyde produced from the concerted path readsorbs on the surface, it can easily dehydrogenate to acetyl (CH_3CO). In fact, even if the CH path is followed, it will also end with CH_3CO, as found previously,[48] for thermodynamic reasons. The CH_3CO-to-1-hydroxyethylidene (CH_3COH) transition is a reversible reaction in the absence of oxidative species (at low potentials). It is noticed that these C_2 intermediates (CH_3CHO, CH_3CO, and CH_3COH) all possess very high barriers for C−C bond breaking (>1.0 eV). At this stage, CH_3CO formation via either the α-dehydrogenation of CH_3CHO or the O−H cleavage of CH_3COH is facile (E_a < 0.15 eV), while CH_3CO decomposition via C−H or C−C bond breaking is highly unfavorable (E_a > 0.96 eV). It indicates that, at smooth conditions (low electrical potentials and low temperatures), CH_3CO may be the deepest oxidation product of ethanol on Pt{111}. This may explain the fact that CH_3CO is an abundant species observed experimentally, although CH_3CO was also suggested to be the precursor for C−C bond breaking.[13−15] We will show later that it is CH_2CO or CHCO that leads to C−C bond breaking at and only at minority surface sites.

Under oxidative conditions where oxidative species such as OH are present (at higher potentials), we found that CH_3CO can further react with hydroxyl easily (E_a = 0.31 eV) to yield acetic acid (CH_3COOH). CH_3COOH can lose its carboxylic hydrogen to become adsorbed acetate (CH_3COO). As shown in Figure 2a, acetate adsorbs in a bidentate configuration with the two oxygen ends bonding to Pt, which is consistent with the structure proposed by experiment using surface-enhanced infrared adsorption spectroscopy.[49] To further oxidize acetate, however, is kinetically prohibited. We have searched the likely routes to degrade acetate, including C−C bond cleavage and C−H bond cleavage with and without the help of hydroxyl. All of them are hindered by reaction barriers greater than 1 eV, although the participation of OH will help the dehydrogenation of CH_3COO to CH_2COO (Figure 2b). Considering that monatomic steps are inevitably present along with terraces, it is essential to know whether acetate can decompose at such minority sites. To this end, we studied the acetate adsorption and degradation on Pt{211}, which contains {100} stepped sites along with {111} terraces. The adsorption structure of acetate is similar to that on the {111} surface (Figure 2a). The most likely oxidation pathway for acetate degradation on Pt{211} also involves hydroxyl as the oxidative agent in dehydrogenation. Although the barrier (0.98 eV) is already lower than that on Pt{111} by 0.20 eV, it is still a bit high for a reaction to take place at room temperature. Further, taking into account the intrinsic low population of stepped sites, it is expected that the acetate oxidation is a slow process, which agrees with the general findings that acetic acid (acetate) oxidation is inhibitive on polycrystalline Pt at ambient temperatures.[12,49,50] Experimentally, it was found that acetate can be totally cleaned off only at highly positive potentials (i.e., above 1 V vs NHE [49,51]). The additional results for acetate decomposition on monatomic steps complete our mechanism on {111}. We can conclude that conventional Pt catalysts that contain dominantly Pt{111} terraces are poor catalysts for ethanol electro-oxidation, as the major products would be acetaldehyde and acetic acid.

(46) Climent, V.; Gomez, R.; Orts, J. M.; Feliu, J. M. *J. Phys. Chem. B* **2006**, *110*, 11344.
(47) Markovic, N. M.; Schmidt, T. J.; Grgur, B. N.; Gasteiger, H. A.; Behm, R. J.; Ross, P. N. *J. Phys. Chem. B* **1999**, *103*, 8568.
(48) Wang, H. F.; Liu, Z. P. *J. Phys. Chem. C* **2007**, *111*, 12157.
(49) Shao, M. H.; Adzic, R. R. *Electrochim. Acta* **2005**, *50*, 2415.
(50) Ma, Z.; Zaera, F. *Catal. Lett.* **2004**, *96*, 5.
(51) Xia, X. H.; Liess, H. D.; Iwasita, T. *J. Electroanal. Chem.* **1997**, *437*, 233.

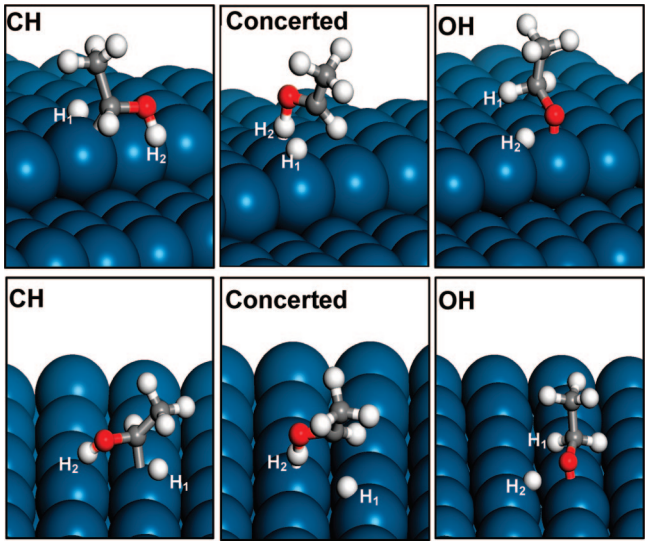

Figure 3. Transition-state structures of initial ethanol dehydrogenation following the CH path, the concerted path, and the OH path on Pt{211} (upper panel) and Pt{100} (lower panel).

The above results allow us to pin down the key bifurcations in the reaction network that controls the selectivity of ethanol oxidation: (i) the initial bond breaking of ethanol and (ii) the oxidation of acetyl. In the former, the key issue is to avoid the concerted path. One has to find ways to force ethanol to follow the stepwise dehydrogenation pathway to chemisorbed C_2 species, instead of weakly adsorbed acetaldehyde. In the latter, acetic acid formation is certainly undesirable, since CH_3COOH cannot be further oxidized to CO_2. A naive solution is to always carry out the reaction in nonoxidative environments, which can prevent acetyl hydroxylation. This is, however, not operative because oxidative species will eventually be essential in order to oxidize C_1 products such as CH_x and CO. The alternative means may involve controlling the kinetics, either by speeding up the dehydrogenation of CH_3CO or by slowing down the hydroxylation process. The next subsection will concentrate on how minority surface sites can modify the kinetics of these two reaction steps.

3.1.2. Pt{211} and Pt{100}. By further examining the two key reaction steps on the monatomic steps {211} and the open surface {100}, we were able to reveal the difference in reactivity between the surfaces.

For the initial bond breaking of ethanol, three pathways on the two surfaces were searched, i.e., the CH path, the OH path, and the concerted path, which are shown to be the most likely reaction channels on Pt{111}. Their located transition states are shown in Figure 3, and the structural parameters at the TSs and the reaction barriers are listed in Table 1. First, we found that the reaction barriers of the CH and OH bond-breaking reactions are reduced on going from {111} to {211} and {100} surfaces. This is consistent with the general rule that surface defects with less-coordinated surface atoms are generally more active for bond breaking.[28,52] We will see in section 3.2 that this rule actually applies to all the other bond-breaking reactions. Second, we found that the CH path becomes the most favorable pathway on Pt{211} and {100}. The barrier difference between the one-step concerted dehydrogenation (E_a^2) and the α-dehydrogenation (E_a^1), i.e., $E_a^2 - E_a^1$, is more than +0.1 eV after the ZPE correction, in comparison with −0.06 eV on Pt{111}. This implies that much less acetaldehyde will be produced on the minority surfaces, Pt{211} and {100}, at low coverages (the high coverage conditions will be discussed in section 4.2.2).

Table 1. Reaction Barriers (E_a) and Structural Parameters of the TSs (Figure 3) for Initial Ethanol Dehydrogenations Following the CH path, the Concerted Path, and the OH Path

	Pt{211}			Pt{100}		
	CH	concerted	OH	CH	concerted	OH
E_a/eV	0.51	0.77	0.64	0.43(0.25)[a]	0.66(0.39)[a]	0.77
$d_{\alpha C-H1}$/Å	1.603	2.082	1.13	1.487	2.010	1.157
d_{C-O}/Å	1.398	1.279	1.440	1.390	1.296	1.413
d_{O-H2}/Å	0.989	1.210	1.713	1.012	1.129	1.675
d_{Pt-H2}/Å	2.878	1.833	1.643	2.446	1.91	1.628
$d_{Pt-C\alpha}$/Å	2.295	3.107	3.077	2.337	3.437	2.829

[a] The data in parentheses are the barriers after zero-point-energy correction.

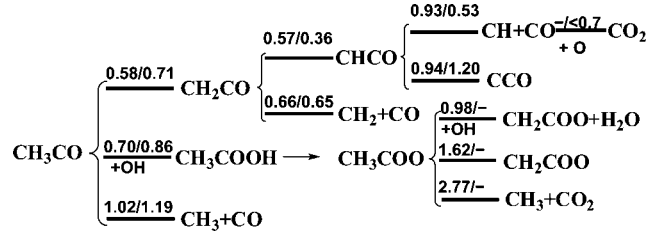

Figure 4. Calculated reaction network and reaction barriers (units, eV) for acetyl oxidation on Pt{211} (data on the left) and Pt{100} (data on the right). H atoms produced are omitted. The barriers not available are denoted as (−).

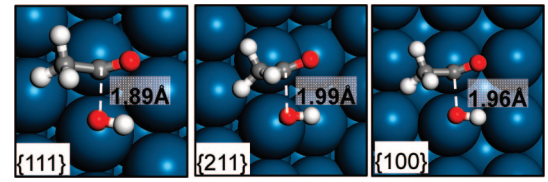

Figure 5. Located TS structures of reaction $CH_3CO + OH \rightarrow CH_3COOH$ on three surfaces.

For the oxidation of acetyl, the reaction pathways on {211} and {100} were determined and are shown schematically in Figure 4. We found that, on Pt{211} and {100} surfaces, the reaction $CH_3CO + OH \rightarrow CH_3COOH$ is significantly inhibited (the TSs are shown in Figure 5), while the dehydrogenation of CH_3CO becomes more feasible. This is in contrast to our findings on Pt{111}, where the selectivity to acetic acid is more favored. Quantitatively, the value of the hydroxylation barrier minus the dehydrogenation barrier increases from −0.65 eV on Pt{111} to +0.12 eV on Pt{211} and to +0.15 eV on Pt{100}.

The overall pathway of acetyl oxidation on Pt{211} can be described as follows. Acetyl adsorbs initially at the top site of the step-edge and dehydrogenates into CH_2CO with a barrier of 0.58 eV, in competition with reaction of CH_3CO with an OH group with a barrier of 0.70 eV (the TS structure is illustrated in Figure 5). CH_2CO can then break either its CH bond or its CC bond with similar reaction barriers of ∼0.6 eV. If the CH bond breaks, the product CHCO is difficult to further decompose because its adsorption configuration at the steps is too stable (see Supporting Information). These results suggest that ethanol oxidation on the {211} monatomic step remains incomplete by producing the stable CHCO intermediate.

(52) Liu, Z. P.; Hu, P. *J. Am. Chem. Soc.* **2003**, *125*, 1958.

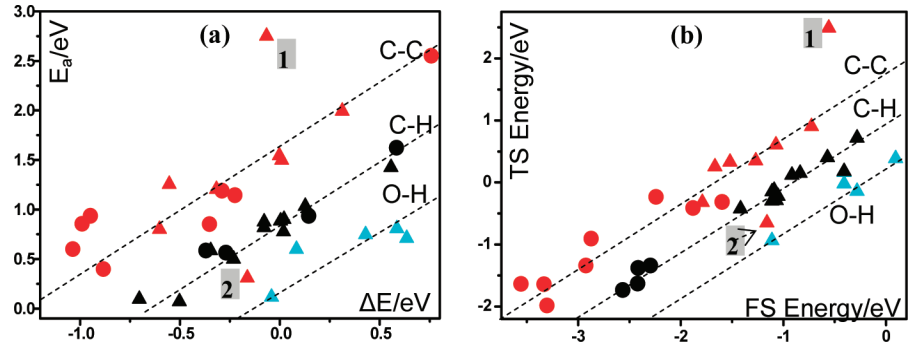

Figure 6. (a) Plot of the barrier (E_a) against the reaction energy (ΔE). (b) Plot of the TS energy against the FS energy for all the bond-breaking reactions studied on Pt{111} (triangles) and Pt{211}(circles). The red, black, and cyan symbols denote the C−C, C−H, and O−H bond-breaking reactions, respectively. The points with the largest deviation correspond to the reactions $CH_3CH_2OH \rightarrow CH_3 + CH_2OH$ (labeled as 1) and $CCOO \rightarrow C + CO_2$ (labeled as 2). (The origin of the deviation is discussed in the Supporting Information.)

On Pt{100}, it is also easier for CH_3CO to dehydrogenate than to react with hydroxyl. The TS of hydroxylation is very similar to those on other surfaces, as shown in Figure 5, in which both fragments CH_3CO and OH reside at atop sites. The lowest-energy pathway of acetyl oxidation on Pt{100} is to lose its two α-hydrogens sequentially to yield CHCO (Figure 4). At that stage, C−C bond cleavage occurs naturally to yield CH and CO fragments with a reasonable barrier ($E_a = 0.53$ eV). The whole process is highly exothermic by nearly 2 eV (see Supporting Information), which implies that the reverse reactions are unlikely to occur. Finally, CH and CO can react with surface O atoms to form CO_2 with reaction barriers below 0.7 eV. It may be noticed that the C−C bond breaking of CH_2CO on Pt{100} is already feasible with a barrier 0.65 eV (Figure 4), which is not, however, the lowest-energy channel, as the dehydrogenation of CH_2CO to CHCO ($E_a = 0.36$ eV) is much easier.

3.2. Thermodynamical Factors in Ethanol Oxidation. The reactions investigated in this work constitute a large database for understanding the chemistry of oxygenated hydrocarbons on metals. For example, we were able to examine the effect of thermodynamics on reaction barriers. We have plotted the reaction barriers against the reaction energies of the bond-breaking reactions on Pt{111} and Pt{211} in Figure 6a (the data set is available in the Supporting Information). Here the reaction energy is defined as the energy difference between the final state (FS) and the initial state, which is close to the reaction enthalpy for surface reactions. The barrier vs enthalpy relationship is known traditionally as the Brönsted−Evans−Polanyi (BEP) correlation. In previous studies, a good linear BEP relationship has been identified for dissociation of gas-phase molecules such as CO and N_2 across different metal surfaces.[53–55] However, for the cleavage of different types of bonds over the same surface, whether the BEP relation holds or not is still unclear.

As shown in Figure 6a, we have identified three distinct regions, each corresponding to a class of bond-breaking reactions. This striking feature simply reflects that no single BEP relation can be established for all reactions on the same surface. The upper-left region is dominated by the C−C bond breaking, the bottom-right region is mainly about the O−H bond breaking, and the area in-between is for the C−H bond breaking. Inside each region, a linear BEP relationship holds roughly for most of the reactions. There also is no obvious distinction between reactions occurring on Pt{111} and those on Pt{211}. As the CC, CH, and OH bonds are known to possess quite different bond polarities, the figure shows that the activity (the barrier height) not only depends on thermodynamics, as represented by the reaction energy, but also is determined by the intrinsic bond polarity. Under similar thermodynamic conditions, the polar bond breaks first. A nice example, as we found in the map, is the three bond-breaking reactions of CH_3COH on Pt{111}, i.e., $CH_3COH \rightarrow CH_3CO + H$, $CH_3COH \rightarrow CH_2COH + H$, and $CH_3COH \rightarrow CH_3 + COH$. They are all almost thermoneutral reactions, while the barrier height follows clearly CC > CH > OH. Except for this, the thermodynamics is often the most important factor in determining the barrier height. The CH bond breaking for an adsorbed species on Pt is usually exothermic, while that of an OH bond, if available, is often endothermic on Pt. The thermodynamics factor determines that the CH bond breaking is usually preferred over the OH bond breaking, although the OH bond is more polar than the CH bond. This is what we found in ethanol oxidation, and what was reported by Desai et al.[56] in methanol dehydrogenation.

4. Analyses and Discussions

4.1. Origin of the Structure-Sensitivity of Selectivity. Among the three surfaces investigated, we have shown that Pt{100} is the most efficient catalyst to fully oxidize ethanol at low coverages. The other two surfaces, by contrast, suffer from the poisoning of stable intermediates that are difficult to further decompose, i.e., acetate on Pt{111} and CHCO on Pt{211}. By examining carefully the two critical steps that determine selectivity, we found that the TS structures of the same reaction are, in fact, very similar over different surfaces. For example, as shown in Figure 5, the TS structures of $CH_3CO + OH \rightarrow CH_3COOH$ on three surfaces share a common feature: both CH_3CO and OH fragments are located at atop sites. This important feature allows us to probe the origin of the barrier change from surface to surface, as discussed below.

4.1.1. α-Dehydrogenation vs Concerted Dehydrogenation. α-Dehydrogenation reactions are very common in ethanol oxidation. Among them, $CH_3CH_2OH \rightarrow CH_3CHOH + H$ (the CH path) and $CH_3CO \rightarrow CH_2CO + H$ are important to

(53) Bligaard, T.; Norskov, J. K.; Dahl, S.; Matthiesen, J.; Christensen, C. H.; Sehested, J. *J. Catal.* **2004**, *224*, 206.
(54) Michaelides, A.; Liu, Z. P.; Zhang, C. J.; Alavi, A.; King, D. A.; Hu, P. *J. Am. Chem. Soc.* **2003**, *125*, 3704.
(55) Liu, Z. P.; Hu, P. *J. Chem. Phys.* **2001**, *114*, 8244.
(56) Desai, S. K.; Neurock, M.; Kourtakis, K. *J. Phys. Chem. B* **2002**, *106*, 2559.

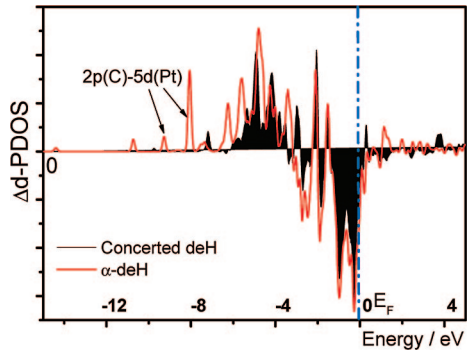

Figure 7. Variation of the *d*-projected density of states of the surface Pt atom due to its bonding with TS complex in α-dehydrogenation and concerted dehydrogenation of ethanol on Pt{111}.

selectivity. These α-dehydrogenation reactions strongly prefer to occur on Pt{211} and Pt{100} in general. On these low-coordinated surface sites, the barrier of $CH_3CH_2OH \rightarrow CH_3CHOH + H$ can be 0.21 eV lower than that on Pt{111}, and that of $CH_3CO \rightarrow CH_2CO + H$ can be 0.38 eV lower. In contrast, the concerted dehydrogenation of CH_3CH_2OH is not so sensitive to surface structure changes. It has similar barriers on Pt{111} (0.65 eV) and Pt{100} (0.66 eV) but a slightly higher barrier on Pt{211} (0.77 eV). Overall, the presence of low-coordinated surface sites can facilitate α-dehydrogenations toward CO_2, which suppresses CH_3CHO production via the concerted dehydrogenation. While the reduction barrier of α-dehydrogenation reactions at low-coordinated surface sites may be rationalized by thermodynamics as shown in Figure 6, it is more intriguing that the two types of dehydrogenation reactions respond differently to changes of the surface structure. The TS electronic structures of the reactions may provide some clues.

We calculated the density-of-states projected onto the *d*-states (*d*-PDOS) of the surface Pt atom on the bare surface and the *d*-PDOS of the Pt atom that bonds with the TS complex (at the TS). As shown in Figure 7, we then plotted the Δ*d*-PDOS of the Pt by subtracting the *d*-PDOS of the TS by that of the bare surface for the α-dehydrogenation and the concerted dehydrogenation of ethanol on Pt{111}. Figure 7 shows that the TS complexes *do* interact with metal surfaces by evolving new covalent bonding: more *d*-states at low-energy regions emerge, together with the depletion of *d*-states around the Fermi level. Quantitatively, eq 8 was used to calculate the stabilization energy (E_d) of the *d*-states due to the presence of the TS complex,

$$E_d = \int_{-\infty}^{E_F} \varepsilon(n_d^{TS} - n_d^{bare})\, d\varepsilon \qquad (8)$$

where n_d is the normalized density of states of Pt (units, electron/eV) with and without bonding with the TS complex and ε is the energy level (eigenvalue). The calculated E_d is −7.4 eV for α-dehydrogenation and −4.5 eV for the concerted dehydrogenation on Pt{111}. This suggests that α-dehydrogenation interacts more strongly with the surface atom than does the concerted dehydrogenation, which agrees with the TS structural features (see Figure 3). For the α-dehydrogenation reactions, the TSs are generally achieved with the C−H bond breaking over one surface metal atom. At the TS, the C-containing fragment (CH_3CHOH) also bonds with the surface, as evidenced by the additional 2*p*(C)-related peaks in Figure 7. On the other hand, the concerted TS involves only H's in close contact with the surface, while the CH_3CHO fragment is far above the surface (see Table 1, d(Pt−C_α)). Since our DFT calculations show that H adsorption on different Pt surfaces has quite similar adsorption energies, it is understandable that the reaction with the TS that interacts with the surface more strongly through an unsaturated C-containing fragment, i.e., α-dehydrogenation, should be more sensitive to surface structure change.

4.1.2. Acetic Acid Formation: $CH_3CO + OH \rightarrow CH_3COOH$. This reaction is perhaps the most important side reaction in ethanol electro-oxidation. In contrast to the α-dehydrogenation reactions, the formation of acetic acid is less favored on the low-coordinated surfaces. It is interesting to ask why. Since the TS structures of the reaction are similar on the three surfaces studied (Figure 5), it is expected that the potential energy surface of reactants (CH_3CO and OH) that determines the energy cost of the reactant moving from the IS position to the TS position is the key to understanding the barrier difference.

Indeed, we found that the barrier height is largely determined by the potential energy surface of OH on surfaces (detailed analyses shown in Supporting Information). On Pt{111}, the OH has a very flat potential energy surface, with the energy difference between the bridge and the atop site being ∼0.1 eV, but the energy costs for OH moving from a bridge to an atop site on the other two surfaces are dramatic, i.e., 0.45 and 0.62 eV on {211} and {100}, respectively. Our DFT results suggest that lower-coordinated surfaces, such as {211} and {100}, tend to bond OH more strongly at bridge sites than at atop sites. This extra energy cost, due to the corrugation of the OH potential energy surface, thus decreases OH activity, since OH must be activated to an atop site to free its 2*p*-states before reacting with other species.[57]

4.2. Mechanistic Implications on Ethanol Electro-oxidation over Pt Catalysts. Understanding the structure-sensitivity of the key elementary steps, we are now in a position to address the mechanism of ethanol oxidation over Pt in the context of direct ethanol fuel cells.

4.2.1. Oxidative Conditions As Pinned by the Electrical Potential. Our mechanism for ethanol oxidation indicates that CO_2 and CH_3COOH originate from the same reaction intermediate, CH_3CO. Therefore, the relative ratio of CO_2 to CH_3COOH should be very sensitive to the oxidative condition, which is related to the electrical potential. The theory here rationalizes the experimental result that the increase of CH_3COOH at elevated potentials (e.g., 0.45 V vs NHE) is at the expense of CO_2 production. We also point out that the other major product, CH_3CHO, is mainly produced from ethanol directly, and therefore the selectivity to CH_3CHO is not so sensitive to the oxidative conditions. This agrees with the experimental observation that CH_3CHO is always the dominant product from 0.40 to 0.70 V.[4]

The current microscopic picture of ethanol oxidation provides an atomic-level interpretation for some elusive concepts in the field. For example, it was suggested by experimentalists[13] that (i) CO_2 formation originates from "strongly adsorbed intermediates" but acetaldehyde comes from "weakly adsorbed intermediates" and (ii) the C−C bond cleavage and subsequent oxidation to CO_2 is a "slow kinetic process". From our results, the "strongly adsorbed intermediates" leading to CO_2 correspond to the adsorbed dehydrogenation fragments of ethanol, such as CH_3CHOH, CH_3CO, and CH_3COH, on the open Pt{100} surface, while the "weakly adsorbed intermediates" are ethanol and the CH_3CHO from the concerted path that occurs on close-packed Pt{111}. The slow

(57) Michaelides, A.; Hu, P. *J. Am. Chem. Soc.* **2000**, *122*, 9866.

kinetics of CO_2 formation is now understandable as a result of the low population of active sites where the C−C bond breaking takes place. The reaction barriers of C−C bond breaking are, in fact, not high, in agreement with the fact that CO_2 starts to form at low temperatures and low potentials.

4.2.2. Surface Coverage Effects. The surface coverage at realistic conditions may be another important factor affecting the selectivity. In experiments, hydrocarbons (CH_x) and CO species were commonly observed at the operating potentials of the fuel cell anode (i.e., below 0.5−0.6 V vs NHE). Although our calculations were performed at low coverage conditions without neighboring coadsorbates, we may still deduce the coverage dependence of the key reaction steps on the basis of our understandings achieved in the last section.

For the initial dehydrogenation of ethanol, we have shown that α-dehydrogenation (CH path) is favored when surface metal atoms are less coordinated. The concerted path to yield acetaldehyde is, in contrast, much less affected by surface structure. Since the coadsorbed species such as CO and CH_x would reduce the bonding ability of surface metal atoms by deactivating the metal *d*-states,[58] the increase of surface coverage is expected to benefit the selectivity toward concerted dehydrogenation. To verify this theory, we have tentatively performed DFT calculations for the initial dehydrogenation of ethanol on a CH-precovered Pt{100} surface where the CH coverage is 0.33 ML. The detailed structures and energetics are shown in the Supporting Information. Indeed, we found that, on this surface, α-dehydrogenation and concerted dehydrogenation of ethanol exhibit almost identical reaction barriers (after ZPE correction), i.e. 0.52 eV, respectively. In the presence of CH, the barrier of α-dehydrogenation increases by 0.27 eV, while that of concerted dehydrogenation increases only by 0.13 eV. This implies that acetaldehyde production, even on Pt{100}, should be greatly enhanced at high surface coverage conditions. Our recent work on Pt{111} also supports this finding, as the preference for the concerted path is not affected, even in the presence of coadsorbed species such as H and H_2O.[48]

It must be borne in mind that, at high surface coverages, C−C bond cleavage should also be retarded. This is because the bond-breaking reactions require extra surface vacant sites to accommodate the dissociated fragments. Lateral interaction at high coverages, often due to the surface-mediated bonding competition effect,[59] will weaken the bonding of the final products more than the initial state and, therefore, reduce the reaction enthalpy in general. Since the dissociation barrier is linearly related to the reaction enthalpy from the BEP rule, the high surface coverage is expected to hinder C−C bond breaking and eventually quench the selectivity to CO_2. From both dehydrogenation and C−C bond-breaking reactions, one can deduce that a good DEFC catalyst must be able to oxidize surface fragments (e.g., CH_x and CO) efficiently.

4.2.3. Catalytic Roles of Minority Sites. We have already shown that the presence of minority sites can suppress the partial oxidation but promote the C−C bond breaking. The dual effects are due to the switches of selectivity in the two key reaction steps at minority sites. Our DFT results are well supported by the experimental findings in ethanol electro-oxidation. For example, Chang, Leung, and Weaver[15] reported that Pt{100} and Pt{110} significantly inhibit acetic acid formation, in comparison with Pt{111}. Tarnowski et al.[28] further proved that the amount of acetic acid produced is inversely proportional to the density of surface steps by comparing ethanol electro-oxidation on Pt{111}, Pt{557}, and Pt{335} surfaces.

Our work suggests that the presence of Pt{111} lies at the heart of the dilemma for ethanol oxidation over Pt. Considering that the {111} surface is the facet of the lowest surface energy in Pt, it is not surprising that commercial Pt-based catalysts, such as Pt/C and polycrystalline Pt, all suffer from poor selectivity in ethanol electro-oxidation. Recent experimental work by Tian et al.[30] shed light on solving the problem. They prepared nonconventional Pt tetrahexahedra nanocrystals (THH NCs) where only {100} terraces and their monatomic steps are exposed (mainly {730} facets). It was revealed that the transient current density of ethanol oxidation on THH Pt NCs keeps increasing during the applied potential range from 0.25 to 0.8 V (vs NHE), while that on traditional Pt nanospheres and Pt/C catalysts drops after reaching a maximum. They suggested that the THH Pt NC materials can overcome the poisoning problem at fuel cell anode operating potentials that the traditionally prepared Pt catalysts experience. From our results, the success of the novel Pt material may be attributed to two reasons. First, it contains only Pt{100} terraces, but not Pt{111} terraces. Second, the presence of a large density of steps should help greatly H_2O splitting to generate oxidative species (OH an O) starting at low potentials, which benefits the oxidation/removal of CH_x and CO species on the surface. This effectively maintains a low coverage to reduce acetaldehyde formation and avoid poisoning.

5. Conclusions

This work represents the first theoretical attempt to establish a comprehensive mechanism for ethanol oxidation on differently structured Pt surfaces in relation to direct ethanol fuel cell applications. The three most typical Pt surfaces, namely close-packed Pt{111}, monatomic stepped Pt{211}, and open Pt{100}, are chosen as model catalysts to address the role of surface structure on the selectivity in ethanol oxidation. To allow for the investigation of a great number of reaction channels, a new transition-state searching method has been developed that implements the bond distance constraint based on a quasi-Newton−Broyden method and updates the constraint progressively to locate the transition state. The current technique enables the location of the transition states, i.e., saddle points, for most reactions as simply and efficiently as the optimization of the stable states (local minima on the potential energy surface).

The detailed reaction network has been mapped out on three surfaces. The theory demonstrates for the first time that the selectivity of ethanol oxidation on Pt is highly structure-sensitive, and Pt{100} is the best surface to fully convert ethanol at low coverages. We show that CO_2 and acetic acid originate from the same surface intermediate, CH_3CO, but acetaldehyde originates from ethanol directly. C−C bond breaking occurs through strongly chemisorbed precursor CH_2CO or CHCO only at low-coordinated surface sites, not from CH_3CO as proposed previously. Acetaldehyde is produced via the one-step concerted dehydrogenation of ethanol, which occurs mainly on the close-packed {111}. Acetaldehyde production is enhanced by the increase of surface coverages such as CH_x. Acetic acid is the dominant oxidation product on Pt{111} at oxidative conditions, but its formation is significantly inhibited by the minority surface sites, which rationalizes the long-standing puzzles in experiment. By detailed analyses, we further identified two fundamental quantities that dictate the selectivity: (i) the bonding ability of

(58) Hammer, B.; Norskov, J. K. *Adv. Catal.* **2000**, *45*, 71.
(59) Liu, Z. P.; Hu, P.; Lee, M. H. *J. Chem. Phys.* **2003**, *119*, 6282.

surface atoms with unsaturated C-containing fragments and (ii) the stability of hydroxyl at surface atop sites relative to other surface sites. Both quantities are related to the coordination number of surface metal atoms.

The DFT results have been analyzed and rationalized in terms of both thermodynamics and kinetics. We show that the linear BEP relation, a thermodynamics rule, holds roughly for different reactions across different surfaces but involving the same type of bond (C−C, C−H, etc.). While the BEP relation lacks quantitative accuracy, it may be used to qualitatively predict the general pattern in dissociation reactions, such as reaction sites and the reaction precursor. The selectivity of surface reactions is determined mainly by kinetics, which can be understood on the basis of a clear view of the transition-state structures.

Acknowledgment. This work is supported by NSF of China (20573023, 20773026, 20721063), Pujiang plan, NSF of Shanghai Sci. Tech. Committee (06PJ14011). Shanghai Supercomputing Center is thanked for computing time.

Supporting Information Available: Illustration of TS-searching trajectories using our constrained Broyden minimization method; CHCO adsorption and decomposition on Pt{211}; potential energy diagram of acetyl oxidation on Pt{100}; ethanol initial dehydrogenation on 0.33 ML CH-precovered Pt{100}; the data set from Figure 6 together with discussion; barrier analyses on the $CH_3CO + OH$ reaction. This material is available free of charge via the Internet at http://pubs.acs.org.

JA801648H